Correlations between Aharonov-Bohm effects and one-dimensional subband populations in $GaAs/Al_xGa_{1-x}As$ rings

J. Liu and W. X. Gao
Department of Physics and Astronomy, The University of North Carolina at Chapel Hill, Chapel Hill, North Carolina 27599-3255

K. Ismail
Department of Telecommunication and Electrical Engineering, University of Cairo, Cairo, Egypt and IBM Research Division, T. J. Watson Research Center, Yorktown Heights, New York 10598

K. Y. Lee and J. M. Hong
IBM Research Division, T. J. Watson Research Center, Yorktown Heights, New York 10598

S. Washburn
Department of Physics and Astronomy, The University of North Carolina at Chapel Hill, Chapel Hill, North Carolina 27599-3255

(Received 21 June 1993; revised manuscript received 2 August 1993)

The Aharonov-Bohm (AB) interference patterns in ring-shaped conductors are usually dominated by random features. The amplitude of the oscillations is random from sample to sample and from point to point on the magnetic field axis owing to random scattering of the electron trajectories by impurities within the wires. We report experiments on devices made with wet etching and global gates, which have shown major progress towards removing the random features. In loops that exhibit ballistic conductance plateaus and cyclotron orbit trapping at 4.2 K, the random pattern of AB oscillations (observed for $T < 0.1$ K) can be replaced by a much more ordered one—especially if only a few transverse modes are populated in the ring. The amplitude and shape of the oscillation envelope function change systematically as subbands are populated in the wires forming the loops. Mechanisms governing the AB effect in the ballistic regime are discussed. Correlation has been found between the $G(V_g,B=0)$ staircase and the beating period of the envelope functions. Quantum oscillations in $G(V_g,B=0)$ are consistent with direct interference of paths of unequal length. Both the correlations and the quantum oscillations in gate voltage are signatures of ballistic transport.

INTRODUCTION

The Aharonov-Bohm (AB) interference effects[1] have been studied extensively in small metallic rings.[2] In these devices, electrons encounter large amounts of elastic scattering and move diffusively. The elastic mean free path is typically $l_e \sim$10–100 Å. The AB effects are observable in these systems because at low temperatures the quantum phase information is retained over a much longer distance l_ϕ, the phase coherence length,[3,4] which can be 3–4 orders of magnitude greater than l_e at temperatures below $T = 1$ K. In metals the electrons are highly degenerate and the Fermi wavelength is much smaller than the diameters of wires that form the loop (typically three orders of magnitude); hence, there are a large number of states on the Fermi surface contributing to the electron transport, and there is no quantization of electron motion in the direction transverse to the wire.

Following the discovery of the quantized conductance in semiconductor heterostructure point contacts,[4,5] much work has been devoted to the study of one-dimensional (1D) electron subbands (or modes) in electron transport.[6,7] The subbands arise due to the low carrier density in semiconductor interfaces, which leads to a long Fermi wavelength, which is, in turn, comparable to the width t of the wire. Both theory and experiments[4–8] have shown that in a straight channel, the conductance contributed by each subband is $2e^2/h$ (2 from spin degeneracy). If the carrier density is controlled by a gate voltage, the conductance will change in increments of the basic conductance quantum to $2Ne^2/h$, where $N = 0, 1, 2...$ is the number of occupied subbands. Recently, AB experiments have been carried out in loops fabricated on high electron mobility $GaAs/Al_xGa_{1-x}As$ heterostructures, and large-amplitude AB oscillations have been reported by several groups.[9–14] Since electron conduction is via the subbands, the subband population ought to affect the AB interference pattern dramatically. If no scattering occurs, and electrons are guided only by the electrostatic confinement that defines the shape of the device and the Lorentz force, we would expect the electron transmission to be very similar to microwave transmission through waveguides, and that changing the electron density would be analogous to tuning the microwave frequency. In a purely ballistic situation, such a device would be a true *solid state interferometer* in a magnetic field.

Consider what happens to the interference when the

0163-1829/93/48(20)/15148(10)/$06.00

mode population changes. At zero magnetic field, conductance $G(V_g,B = 0)$ is a mode-counting staircase in V_g. In the plateaus, the modes are well defined (transverse momentum is the conserved quantum number), and in the regions linking plateaus new modes are just turning on. At low enough magnetic fields, we may suppose that the field does not alter the subband population substantially. Correlations should be expected between AB oscillations at fixed gate voltage $G(V_g$=const,$B)$ and the mode-counting staircase $G(V_g,B$=0): for V_g on the plateaus of the mode-counting staircase, the AB oscillations are larger and more ordered than V_g in the regions linking plateaus. As a result, the large ordered and somewhat small and disordered patterns will appear alternatingly in the AB oscillations as we sweep the gate voltage. At the same time, we also expect that as more and more modes are populated the structure of the AB effect will become more and more complicated. This can be understood in analogy with a waveguide operated in a single-mode (or few-mode) transmission and in multi-mode transmission. Earlier experiments,[14] however, failed to confirm the expected correlations. Apparently, the interference pattern was dominated by random scattering from donors and surface defects,[6,7] and our ballistic picture simply does not apply. (An exception occurred at *high* magnetic fields in the regime of the quantized Hall effect, where beautiful regular oscillations were observed from a single point contact and from open cavities bounded by point contacts in the transition between two successive Hall plateaus.[7])

This paper will report the results from devices in which scattering has been eliminated to a large degree. Correlations have been found between AB interference patterns and subband population. In addition, quantum oscillations were seen in $G(V_g)$ at $B = 0$, which are consistent with direct interference of paths of unequal length. These are signatures of pure ballistic transport, and so our results contain an encouraging step toward the ultimate goal of completely ballistic devices.

EXPERIMENT

Our samples were fabricated on a standard high-mobility $GaAs/Al_xGa_{1-x}As$ modulation-doped layer ($x = 0.3$, carrier density $n_s = 2.3\times10^{15}/m^2$, and mobility $\mu = 90\ m^2/V\ sec$) grown by molecular beam epitaxy. The ring geometries were defined by shallow trenches formed through a wet etching technique. Metal gates covered all active portions of the devices. We attribute the excellent quality of these devices directly to the softness of the etching and screening effect of the global gate. The effect of the gate in reducing the long-range interaction of ionized dopants should not be underestimated. More details of the fabrication are reported elsewhere.[15] An earlier paper by the authors discussed an experiment on a similar single-ring device at $T = 4.2$ K. Although that temperature was too high to see any AB oscillations, cyclotron orbit trapping was observed, which, in turn, is convincing evidence of substantial ballistic transport in the device.[16]

The samples were a single ring and two and four coupled rings. The lithographic geometry for the coupled two rings is illustrated in Fig. 1. The two parallel rings share one arm. The four-ring sample is the obvious extension of the series with four parallel rings. The rings in all the samples are of the same size. The lithographic pattern has the average radius of $r = 0.8$ μm and linewidth of $t = 0.4$ μm. Previous analysis of the data in similar samples leads to a more realistic estimate of the width of the conduction channel to be $t = 0.3$ μm.[16] The temperature at which the data was taken was 0.04 K unless specified. This temperature is in the regime of large phase coherence length, where interference effects are quite apparent. The resistance was measured through the standard low frequency ac technique with PAR 124A lock-in amplifiers and Ithaco 1211 or 1212 current amplifiers. The excitation voltage ranged from 1 μV to 4 μV at a frequency of 13 or 278.5 Hz. During the measurements, the samples were immersed in the mixing chamber of the dilution refrigerator to ensure good thermal contact.

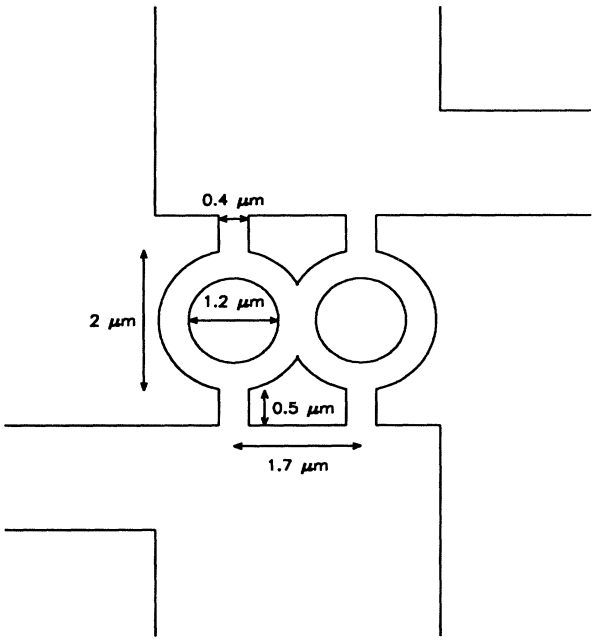

FIG. 1. Schematic drawing with lithographic dimensions for a two-ring sample. The loops and ports are to scale, but the large area regions are not. The region comprising the rings and the ports is covered by a Ti/Au gate.

ANALYSIS OF THE MAGNETORESISTANCE

In Fig. 2, curve *b* displays magnetoresistance for the single ring in a "random" state. At this V_g, there are ~4 filled subbands [judged by the conductance $G(V_g,B$=0), which is not shown] in the ring. The interference pattern in this state is similar to the data from earlier experiments in heterojunctions,[9–14] and also from diffusive metallic loops[2]—namely, rather weak oscillations, and the phase and amplitude of the oscillations are uncorrelated from point to point along the magnetic field axis. The je/h (j is an integer)

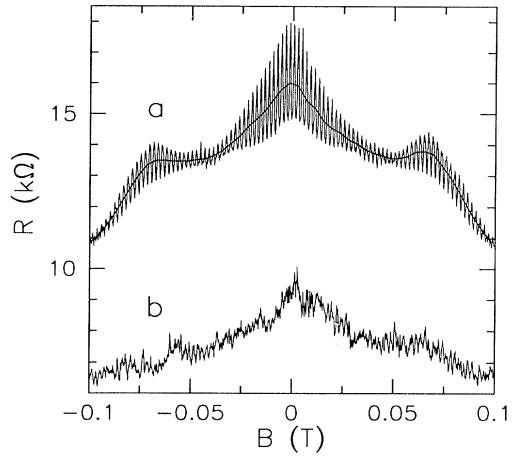

FIG. 2. The magnetoresistance for the single ring at the gate voltage of V_g=0.15 V (a) and V_g=0.24 V (b). The smooth line through the 0.15-V data is the background resistance (its reciprocal is G_0 which will be used later), calculated by averaging the original data in 0.005 T intervals. The peaks near ±0.07 T are due to trapping of cyclotron orbits.

Aharonov-Bohm frequencies are mixed with considerable amounts of other "frequencies" of oscillation yielding a random amplitude for the AB oscillations. In the random state, no correlations among the data at different V_g or between the AB oscillations and the $G(V_g,B=0)$ staircase are apparent.

In Fig. 2, curve *a* displays magnetoresistance data for the single-ring sample in the "ordered" state. $V_g = 0.15$ V, which corresponds to having one filled spin degenerate subband in the ring. In contrast, it is dramatically different from the bottom curve, and from what has been observed typically in the metal rings by many authors,[2,17] and also from the previously reported results in GaAs/Al_xGa_{1-x}As heterostructure rings.[9,11,13] There is a strong correlation in the oscillation phase and amplitude throughout the magnetic field range. This implies that the scattering events are "gentle" in the sense that backscattering is largely eliminated. A small amount of forward scattering to mix the modes is necessary to accomplish the interference process, but it does not appear to corrupt the interference pattern. The latter prospect is consistent with the disappearance of noise in filled subbands.[18,6] Different sweeps at the same gate voltages are in good agreement. The reproducibility of two traces at a fixed V_g is 99% with a time delay of 5 h between the up and down traces in magnetic field, which is comparable to earlier work on GaAs/Al_xGa_{1-x}As.[9] If we use the same data and subtract the smooth background (see below), the envelope of the h/e oscillations, which account for ~ 5–15 % of the total conductance, has a reproducibility of 70–90 %.

The exact reason that the devices get into one or the other state is not clear yet. A more systematic study of device processing and low-temperature transport is needed. It is suggestive that under conditions where good plateaus exist in $G(V_g,B=0)$, the AB effect is cleaner. For two of the samples used in this paper, the initial cooling (300 K to 0.04 K) obtained noisy data, one with very active time-dependent conductance fluctuations on the time scale of seconds, which almost totally buried the AB effect (nevertheless, reasonably good conductance plateaus were seen at $T \sim 1$ K in the same cooldown). After bringing the samples to 300 K *in the dark* and recooling back to 0.04 K, the *same* sample was in a quiet, ordered state, and clean AB oscillations were then observed. Once the sample is in the ordered state, it is fairly stable unless it is raised to a very high temperature ($\gg$4.2 K) or suffers an electrical shock. Based on the theory and experiments on universal conductance fluctuations, this is not so surprising, because only a few active impurities are enough to kill the correlations and even the AB effect itself,[19] even when transport through most of the conducting channel is ballistic. The regions near the ports are especially critical and an inconvenient impurity configuration there can have a huge effect,[20] and this is just the region where the strongest electric fields appear during transport experiments. So we speculate that the above randomness and changes from ordered to random states is related to the movement of a few impurities or defects, probably near the ports. With the view towards the ultimate goal of pure quantum waveguides, these results imply that the task is even more formidable. Not only a very clean channel is needed, but also the elimination of all backscattering within $\sim l_\phi$ of the ports.

Each trace (random or ordered) can be described by a field-dependent smooth background resistance summed with Aharonov-Bohm oscillations of frequencies h/e, $h/2e$, and so on. The background resistance (the smooth line through the oscillations of curve *a* in Fig. 2) is calculated by averaging the original data in every $\Delta B = 0.005$ T interval of magnetic field. This background resistance can be attributed to two parts. One is the overall parabolic component, which we believe to be the magnetic steering of electron away from head-on collisions with the inner wall of the ring. Other physics might contribute, however—for instance, the electron-electron interactions can cause a similar negative magnetoresistance.[21] The electron-electron interaction should be strongly enhanced by the 1D nature of the transport, but (perhaps) suppressed by the screening from the gate and complicated by the donor charges.[22] The cause of the large negative magnetoresistance will not affect the analysis to follow. The second component of the smooth background resistance comprises the broad peaks at ~ ±0.07 T, which agree well with a model of trapped classical orbits in the loop.[16] The peaks in resistance arise when the cyclotron orbit of an individual mode matches the size of the ring, so that the electrons in that mode are guided away from the outlet port and remain in the ring. A peak appears for each individual value of forward momentum, i.e., for each occupied transverse mode, so at the same Fermi energy more than one trapping peak could be seen. In this figure the trapping peaks, except for being dressed by the AB oscillations, are not different from the equivalent data taken at high temperatures. The lack of temperature dependence provides further support for our semiclassical trapping picture, and rules out interference-related models for this

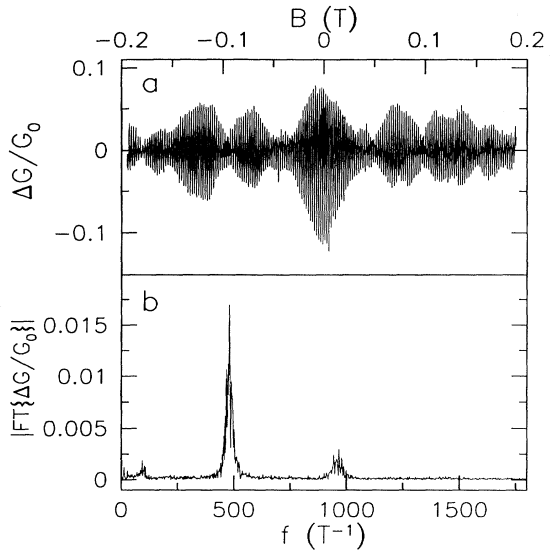

FIG. 3. (a) $\Delta G/G_0$ is the relative conductance oscillations calculated by subtracting the averaged (heavy) line from curve *a* in Fig. 2. (b) The Fourier transform amplitude of $\Delta G/G_0$ from (a).

resistance enhancement.

To be able to see the AB oscillations better, the smooth background G_0 (reciprocal of the dark line) has been subtracted from the original conductance in Fig. 2. Since we will compare the AB effect from a wide range of V_g and B, in which the background itself changes (typically) by a factor of 5, we will study the relative conductance change $\Delta G/G_0$, and this relative conductance oscillation for the top curve in Fig. 2 is shown in Fig. 3(a). (Fig. 2 is cut to ± 0.1 T to show the detailed structure of oscillations.) The envelope function here is mainly from the contribution of h/e frequency. The average spacing between two adjacent nodes is 0.07 T, spanning about 34 fundamental AB oscillations.

It is straightforward to realize that even in the ideal case when absolutely no random scattering is involved, the envelope function will *not be featureless*; instead, it will be governed by some physics which was not emphasized in the diffusive case. First, due to the finite width of the ring arms, different modes with different *transverse spatial* distribution will encircle different amounts of flux and, therefore, have different AB frequencies. A simple calculation of the flux difference between the first and second mode in a square well leads to a result $\sim \pi(r_o - r_i)^2 B/4$, where r_o and r_i stand for the outer and inner radii of the ring. For our geometry we estimate a 4% difference between the two frequencies, and for higher modes our simple argument will give a somewhat smaller result. The result of the composition of two close frequencies is periodic beating of the oscillation amplitude rather like that in Fig. 3(a). If we attribute the change in amplitude to such a mechanism, then typical h/e frequencies differ only by $\sim$ 3%, which is in reasonable agreement with our estimate. From this point of view, Fig. 3(a) is very close to what we can see from an ideal solid state interferometer. We note, however, that even when only one mode is populated there is still some beating of the interference amplitude, although over a longer field scale. Another more plausible explanation is directly related to the cyclotron orbit trapping. When the electron is guided away from the outlet, the amplitude of the oscillations, which results from interference of trajectories escaping the ring, will be suppressed too. As a result, a node will develop in the AB oscillation amplitude accompanying a trapping peak in the resistance. This naive model is not completely supported by curve *a* in Fig. 2, where the envelope nodes do not line up with the trapping peaks, but the average period is approximately correct.

Ordered data such as curve a in Fig. 2 occur at specific values of V_g, while at other V_g the data are not as satisfying, but as long as the sample stays in the quiet state, the typical data are much more ordered than the random case (curve *b*) in Fig. 2. So we generally characterize our "ordered" data as in an intermediate scattering regime, where analysis of the envelope functions based purely on ballistic transport is not entirely adequate. But, as we will see, statistical methods are appropriate and useful in this special regime.

COMPARISON WITH MODE-COUNTING STEPS

Before using more sophisticated methods, we will look at the Fourier transform (FT). Figure 3(b) shows the FT amplitude of the data in Fig. 2(a). Since the smooth background has been subtracted, the zero frequency component in the FT spectrum is not present. The effective cut-off frequency$(1/\Delta B)$ due to this filtering is $\sim$200 T^{-1}. To compare the FT spectrum with the mode-counting steps, systematic measurements have been conducted for the double-ring sample.

In Fig. 4 the zero-field conductance G versus V_g at the temperatures 2 K, 0.74 K, and 60 mK is shown. The conductance staircase is clearest at 0.74 K. The quan-

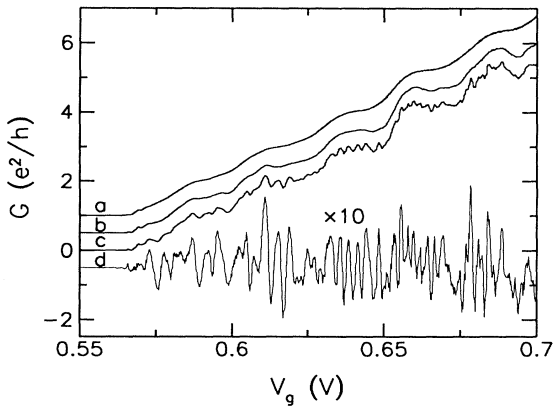

FIG. 4. $G(V_g)$ at several temperatures and B=0 recorded upon a second cooldown with a considerably shifted threshold voltage. The temperatures for the curves are *a*: T=2 K, *b*: T=0.74 K, and *c*: T=0.06 K. The difference between *c* and *b*, which is attributed to interference effects from changing k_F, is plotted as *d*.

tized conductance height is $\sim 1.3e^2/h$. As discussed previously,[15,16] the conductance step does increase with the number of parallel rings in the sample and is *reproducible* from sample to sample with the same geometry. In addition, we notice that the step height $0.75e^2/h$ from the single ring is very close to the the classical addition of two-ports and two-ring arms ($2e^2/h$ each), which would be $\frac{4}{5}\,e^2/h$. But why the classical conductance addition rule should be applicable here is an open question. The clear conductance staircase (sometimes up to nine plateaus) suggests adiabatic coupling between the ports and the ring, which should lead to larger step height than the classical value. On the other hand, the (parallel) ring arms support the same number of modes as the inlet ports, so the arms are "underutilized" as transport paths.

At 60 mK an oscillatory feature dresses the staircase. The oscillations in $G(V_g)$ always accompany the AB effects. At temperatures where the staircase was smooth ($T > 1$ K), no (or very small) AB oscillations were observed. In this figure, we also show the 60-mK data after subtracting the 0.74 K sweep. The average magnitude of the $G(V_g)$ oscillations agrees with the magnitude of the AB effects at a given temperature. This leads us to relate the $G(V_g)$ oscillations to quantum interference.[3] These features differ from the AB effects in that they are not caused by the magnetic flux; they are related, instead, to the change of the Fermi wavelength with changing electron density. From the AB effects, we know that the dominant contribution to the interference oscillations is from the fundamental h/e signal. This frequency results from partial waves from the two ring arms interfering at the outlet. If there is a difference in the two arm lengths, when the Fermi vector changes, the phases accumulated on the trajectories through each arm will be different, the difference being $\Delta l\,\Delta k_F$.[3,14] The average period of the coherence oscillations in $G(V_g)$ is $\Delta V_g = 3$ mV. Using our previous Shubnikov–de Haas measurements of Fermi energy in similar samples,[16] we have estimated that the corresponding change in Fermi wavelength is $\Delta k_F = 40\ \mu\text{m}^{-1}$. From $\Delta l \Delta k_F = 2\pi$, we have $\Delta l/l = 2\pi/(\Delta k_F \pi r) \sim 6\%$, or $\Delta l = 0.15\ \mu$m. This is certainly plausible. The existence of so many oscillations (about 30 total), however, implies that the simple picture above must be modified, since it would account for about ten oscillations at most. If the modes are distinct within the wire then each subband can contribute separate oscillations, which is consistent with the increase in the number of oscillations per plateau as more subbands are populated. Another possibility is that of Fabry-Perot interference between the inlet and outlet ports, which has been reported in similar structures.[23] Further experiments are required to sort out the detailed explanation as well as the rest of the phenomenology.

In Figs. 5(a) and 5(b) we show the Fourier spectrum of the relative AB oscillations at a series of gate voltages. The surface represents 32 magnetoconductance measurements equally spaced between V_g=0.5975 and 0.6700 V and interpolation between successive curves. Three peaks (h/e, $h/2e$, and $h/3e$) are clearly seen throughout the range of gate voltage, and the $h/4e$ peak can be seen at high V_g. The average frequencies for the first three peaks are $506.6 \pm 6.4\ \text{T}^{-1}$, $1011 \pm 11\ \text{T}^{-1}$, and $1511 \pm 18\ \text{T}^{-1}$, respectively, which scale fairly linearly with the harmonic order, as expected. To obtain the frequencies, each harmonic peak at a specific V_g is fitted with a Gaussian. There is *no* systematic dependence of the frequencies on V_g for any of the peaks. These frequencies are typically larger than corresponding frequencies from the single ring, where h/e oscillation is at $f = 482.2\ \text{T}^{-1}$. We speculate this is due to the widening of the ring at the shared arm region between the two rings.

In the same figure we include a panel at the left con-

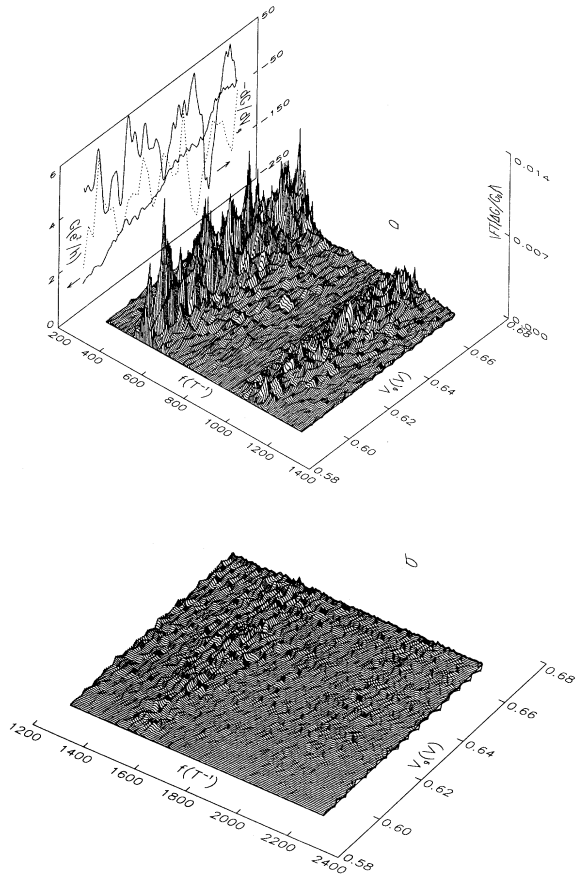

FIG. 5. The Fourier transform of $\Delta G/G_0$ as a function of gate voltage for the double-ring sample, in frequency ranges from 300 to 1300 T^{-1} (a), and 1300 to 2300 T^{-1} (b). The vertical axis in (b) is the same as for (a). The surfaces are constructed from 32 equally spaced measurements between V_g=0.59 V and V_g=0.67 V recorded on the second cooldown. Four peaks are seen at the frequencies $506.6 \pm 6.4\ \text{T}^{-1}$, $1011 \pm 11\ \text{T}^{-1}$, $1511 \pm 18\ \text{T}^{-1}$, and $\sim 2020\ \text{T}^{-1}$. The $G(V_g, B{=}0)$ and (the negative of) its derivative $-dG/dV_g$ (in $\Omega^{-1}\,\text{V}^{-1}$) versus V_g are drawn on the z-y panel and compared with the skyline (dotted line) consisting of the highest points from h/e peaks. The correlation between the mode population and the height of the h/e peak is obvious; there are four main "hills" in h/e and the same number of peaks in $-dG/dV_g$. The strongest h/e oscillations are found around the conductance plateaus, i.e., the zeros of $-dG/dV_g$.

taining $G(V_g)$ at 0.06 K and for comparison, the (negative of the) transconductance $-g_m = -dG/dV_g$ has also been plotted in the same frame. In $-g_m$ the plateaus of G correspond to zeros between -50 and 50, and the regions linking plateaus appear as valleys. In this range of V_g the conductance $G(V_g)$ increases from $\sim 0.94e^2/h$ to $\sim 4.2e^2/h$, corresponding to switching on of modes 1–4. We can see that despite the large change in $G(V_g)$, the average relative AB oscillation $\Delta G/G$ for h/e is approximately constant (although there are order of magnitude fluctuations), implying that the contributions to h/e frequency from each mode are about the same. In contrast, there is a slight increase in $\Delta G/G$ with V_g for the higher harmonics, especially $h/4e$. In principle, this is not expected. At low V_g our resolution in ΔG decreased because the detected current was smaller, so it is possible that the apparent increase in the fourth peak is an instrumental artifact. Other possible explanations include a longer phase coherence length at higher V_g or an effect of the intermode scattering when many modes are populated.

For the h/e frequency, there is an obvious correlation [four main peaks in the Fourier transform lying approximately in line with the four plateaus in $G(V_g,B=0)$] between the spectral density and the population of the modes. For ease of viewing, we also include the projection of all the h/e peaks onto the panel (dotted line), i.e., a "skyline" consisting of the highest points at each V_g. From the graph it is evident that when the $B=0$ conductance is at the center of a conductance plateau, the AB oscillations are stronger, and on the region linking plateaus weaker.

Now examine the scattering processes when a new mode is turned on. Because the subband bottom mainly comprises states with small k, it is sensitive to imperfections of the conducting channel. As a result, the scattering is stronger when a mode is newly populated, which is the reason for the finite width of the regions linking plateaus in V_g. According to the Landauer formula, small angle, intraband scattering has very little effect on the conductance. So we see that the regions linking plateaus are merely manifestations of heavy interband or large-angle intraband scattering (generically called backscattering). Both of these will reduce the h/e AB oscillation size (their roles in general, and for $h/2e$ will be discussed later). Following this line of thinking, we expect a good staircase in $G(V_g,B=0)$ (not counting the fine interference pattern in curve d in Fig. 4) to foretell observation of a periodic oscillation of the scattering strength, and an observation of a correlation between $G(V_g)$ and the AB magnitude is thus *inevitable*. The lack of observation of such correlations in earlier experiments in heterojunctions is consistent with the absence of a clear zero B staircase in their experiments.[9–14] The above analysis is based on a static scattering potential, and not time dependent events which may serve as a phase-breaking source but not a conductance killer (e.g., spin-spin interactions). In this case we may see a staircase at $T \sim 1$ K, but at lower temperatures might not be able to observe any correlations in the AB effect (or, in fact, any phase coherent response at all). This may be the reason for poor AB oscillations in the random state (see above).

The discussion in the last paragraph implies that the quality of correlation closely depends on how clean the staircase is. We note that the low-temperature oscillations at $B=0$ (curve d in Fig. 4) contribute a significant amount to the conductance ($\sim$10%). The nonideal correlation may be attributed to the substructures in the curves of Fig. 4. One should in principle self-consistently model the AB interference patterns with the dressed $B=0$ transmission coefficient.[3]

As a final remark we note that if, starting in Fig. 5 at a peak in the FT at h/e frequency, we move towards lower or higher V_g or B, the peak height decreases smoothly while the peak position drifts. As a result, rather than uncorrelated random spikes, hills with significant footprints are seen. The gate voltage correlation range among the hills is $\sim$ 20 mV, which is about the change required to turn on a new mode. This correlation with gate voltage may be a manifestation of the response of a particular mode evolving its detailed charge distribution as V_g changes, but more detailed investigation of this physics is required. Another consequence of the frequency shift is that the peaks move as V_g changes, so if we show a cross section at any particular f, the global correlation seen in Fig. 5 will *not* be apparent. For the higher harmonics ($h/2e$, $h/3e$, and $h/4e$), no obvious correlations can be seen between the peak heights and the plateaus in $G(V_g,B=0)$.

ANALYSIS OF THE ENVELOPE FUNCTIONS

Besides studying the magnitude of the AB oscillations, we also investigated the patterns of the envelope functions with respect to the subband populations. Similar data have been discussed previously for the disordered (metallic) limit.[2] One expects the interference contribution to the conductance to be of the form[3,24]

$$\Delta G = \sum_{j=0}^{\infty} G_j(B,V_g)\cos\left[\frac{2\pi j\Phi}{(h/e)} + \alpha_j(B,V_g)\right], \quad (1)$$

where Φ is the average amount of magnetic flux enclosed by the electron trajectories encircling the ring, while G_j and α_j are the envelope function and phase that account for individual harmonics. Information about the details of the scattering are contained in G_j and α_j while the oscillatory components contain only the size of the ring. For metal samples these functions have been random in B. The correlation scale for an envelope function G_j is B_c, which, in the diffusive case, is just the field scale to introduce a flux h/e into the sample (i.e., the ports and the arms of the ring). But this diffusive description for B_c does not apply to our data because, even though the effective width of the wire does increase with V_g, it is too small [only 40% (Ref. 16)] to account for what we have observed in our samples; in addition, for our data the B_c changes periodically rather than monotonically (see below). Here we will borrow this vocabulary, such as envelope function G_j and correlation field B_c, to describe our data, and we will explore the degree of "order" in

the envelope functions G_j through their autocorrelation functions.

Now consider the two contrasting curves in Fig. 2 first. In order to analyze the envelope G_1 for the h/e oscillations, we use a Gaussian filter and reverse Fourier transform each h/e peak back into B space. Figure 6(a) illustrates the result for h/e oscillations from the spectrum in Fig. 3(b). The h/e signal accounts for about 80% of the total oscillation magnitude in Fig. 3(a). To ensure that the information in the chosen peaks is fully included, generous filters of half-width 100 T^{-1} around the center frequencies were used. These are at least three times bigger than the widths (15 T^{-1} and 30 T^{-1}) of the h/e and $h/2e$ peaks calculated by fitting Gaussians to the peaks. To reaffirm the validity of the filter, we have done a FT for Fig. 6(a). If we plotted the result in the same picture with 3(b), no difference could be seen between these two curves in the region ± 100 T^{-1} around the center frequency. The same filter width was used throughout the analysis. The same operation for the bottom curve in Fig. 2 obtains the result in Fig. 6(b). Both curves contain AB oscillations of the same average frequency. The differences between the two curves are in correlation scales of the envelope functions G_1 (dark curves that bound the oscillations).

In Fig. 7, we have calculated the autocorrelation functions (solid lines) for G_1 in Fig. 6. The huge difference between the two envelopes is reflected here. For envelope 6(b), the oscillation amplitudes at a particular value of B are not correlated with those at other places on the B axis, so its autocorrelation function for the envelope [7(b)] is mainly Gaussian-like: a single monotonically decaying peak signifying random correlations. The long-dashed line is the autocorrelation function calculated from the average value of the envelope, which is consistent with the constant offset. In contrast for envelope 6(a), a much more regular envelope function seems to prevail. The autocorrelation function for this envelope contains a decaying peak and *a regular* oscillatory "tail," which indicates a nonrandom pattern in the envelope function.

In general, the shape of the correlation function can be understood as follows. Because the envelope function basically consists of the sum of two parts, $G_1(B) = P(B) + Q(B)$, where $P(B)$ is a periodic function, and $Q(B)$ a random function. The autocorrelation function of $G_1(B)$ can then be calculated as

$$\begin{aligned} C(G_1) &= \int [P(B) + Q(B)][P(B + \Delta B) \\ &\quad + Q(B + \Delta B)]dB \\ &= C(P) + C(Q) \\ &\quad + \int [Q(B)P(B + \Delta B) + P(B)Q(B + \Delta B)]dB \\ &= a\cos(2\pi B/B_{c1}) + c\exp(-B^2/B_{c2}^2) + \text{const.} \end{aligned} \tag{2}$$

In the derivation, we have assumed that $P(B)$ and $Q(B)$ are uncorrelated, so the cross term only contributes an insignificant constant. The autocorrelation for $P(B)$ is simply a cos function, $C(P) = a\cos(2\pi B/B_{c1})$; and for the random function $Q(B)$ a Gaussian $C(Q) = c\exp(-B^2/B_{c2}^2)$. The final constant is from all three terms [cross term, $C(P)$ and $C(Q)$], since both $P(B)$ and $Q(B)$ have nonzero average values. B_{c1} is the "beating" period, and B_{c2} the random correlation scale. We acknowledge that there are some problems associated with performing the calculation in a finite field range. The

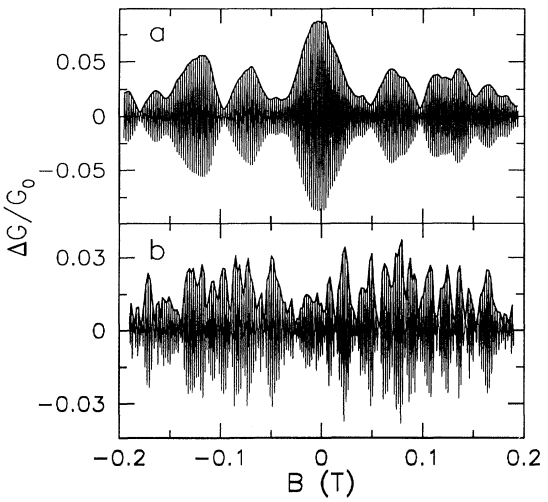

FIG. 6. Inverse Fourier transforms of the h/e peaks are calculated to obtain the oscillation patterns for the upper (a) and lower (b) curves in Fig. 2. The two patterns are defined by different amplitude envelope functions $G_1/G_0(B)$, which are drawn as the smooth dark lines along the oscillation maxima.

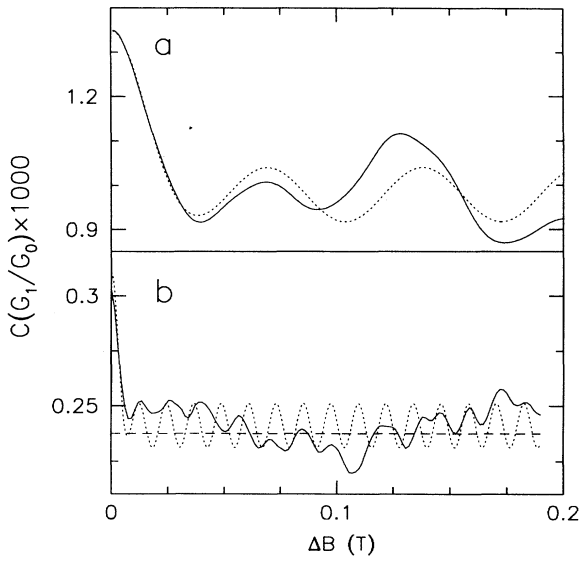

FIG. 7. The measured autocorrelation function (solid line) of the envelope functions G_1/G_0 for the single ring for (a) the upper curve and (b) the lower curve in Fig. 6. The dashed line in (b) is the autocorrelation function calculated from the average value of the envelope, which is consistent with the constant background offset. They are fitted with Eq. (2) (dotted line) to obtain the beat periods B_{c1} and decay scales B_{c2}.

consequence is that none of the above three terms would be ideal; the random function $Q(B)$ will produce oscillatory features in both the cross term and the Gaussian term. This is clearly seen in Fig. 7(b); there are oscillatory features in the tail, which would disappear if the field range were long enough. But we also realize that if the correlation B_{c2} does not exceed the long-range correlation field B_{c1}, only $C(P)$ gives the long-range correlation field B_{c1}.

If we use Eq. (2) to fit the two correlation functions in Fig. 7 (dashed lines), it yields B_{c1}=0.069 T, B_{c2}=0.015 T for curve *a*, and B_{c1}=0.012 T, B_{c2}=0.0030T for curve *b*. $C(Q)$ is restricted to small ΔB; on the other hand, $C(P)$ persists to large ΔB. Here the beating period B_{c1} represents the long-range order of the envelope function. For both curves we can see that the fitted B_{c1} are consistent with the periods we get from the original envelope functions in Fig. 6. So the beating period B_{c1} can be used as a parameter to characterize the order of the envelope function quantitatively. Even for the metallic case 7(b), which is outside the realm of validity for formula (2), the fit yields correctly, at least qualitatively, a very small value of B_{c1}, but the fit quality is rather poor, indicating that there is no long-range order in this correlation function. In the very ordered cases such as 7(a), there might be an even longer B_{c1} if the measurement was extended to a wider range of field, because the window size ±0.2 T puts an upper limit of 0.2 T on B_{c1}. Unfortunately, this cannot be done because depopulation of the subbands and Shubnikov-de Haas oscillations and finally the quantized Hall effect set in, and they cause dramatic changes in the physics behind the AB oscillations, which goes beyond the physics that this paper set out to study.

We have performed the same calculation for all three samples. We notice that for coupled rings (two rings and four rings), Eq. (2) does not always fit the data, and the discrepancy worsens as more modes are occupied. Representative data from the two-ring sample at V_g = 0.660 V are shown in Fig. 8. The autocorrelation function (solid line) contains two oscillation periods. Obviously, a single beat frequency is not adequate in these cases. Instead of invoking a more complicated model, we will keep using (2) to fit the original data by seeking a local minimum in the sum of squares of differences starting from different initial conditions. This method yields the two beat frequencies as shown (dotted and dashed lines) in Fig. 8, where the two periods are 0.081 T and 0.019T, respectively. The average beating periods B_{c1} for G_1 of the three samples are collected in Table I. In cases where two frequencies exist, they were considered with equal weight in the statistics.

TABLE I. Envelope function oscillation scales.

Sample	$\overline{B_{c1}}$	Number of V_g	Mode range
one ring	0.078 T	8	1 → 2
two rings	0.045 T	15	1 → 2
	0.038 T	32	1 → 4
four rings	0.037 T	8	1 → 2

From this table, we can see that, in the same mode population range, the average beat period tends to decrease as the number of rings increases. For the two-ring sample, the only sample for which a relatively wide mode population range was measured, the average beat period tends to decrease as more modes are populated. Among all the samples, only the data from the two-ring sample allow us to make a detailed comparison between the AB effect and $G(V_g, B$=0). The beating periods for h/e oscillations are summarized in Fig. 9(b). In the calculation the fitting results are constantly checked "by eye" against the original envelopes to make sure that the fit re-

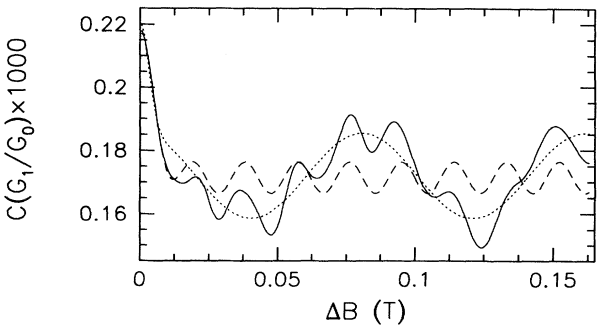

FIG. 8. The autocorrelation of G_1/G_0 for the double ring (solid line) at V_g=0.660 V (second cooldown). It contains more than one beat frequency. It was fitted with formula (2) with different initial conditions to obtain the periods 0.081 T (dotted line) and 0.019 T (dashed line).

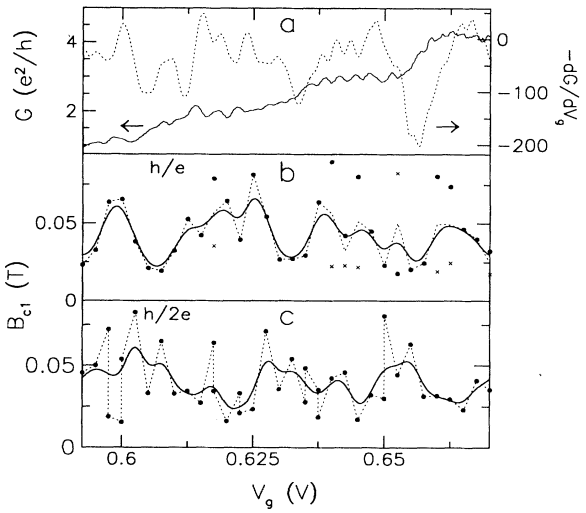

FIG. 9. Comparison between the mode-counting staircase $G(V_g)$ (solid line) and transconductance $-dG/dV_g$ (dotted line) recorded at B=0 (a) and the beat periods for the h/e (b) and $h/2e$ (c) peaks from all of the measurements from Fig. 5. In (b) when two periods are found for a single correlation function as in Fig. 4, the extra one is shown as x. The dashed lines connect the beat periods (the average in cases where there are two). The solid line is a smooth (Gaussian filtered) version of the dashed line. In (b) there is a correlation to the staircase similar to that seen in Fig. 5 for the h/e amplitude of the oscillations. In (c) the opposite trend to (b) is seen.

sults are reasonable. The biggest and the smallest period differ by almost an order of magnitude. In cases where two periods exist, the extra one is plotted as an x. The dashed line connects all points (in cases where there are two points, the average is used) together, and the solid line is a smoothed rendition of the dashed line. Again $G(V_g)$ and $-g_m$ are shown in Fig. 9(a). On the plateaus, the correlation functions have relatively long periods B_{c1}, and shorter periods on the regions linking the plateaus, which coincides with the relationship between FT peak amplitude and $G(V_g,B=0)$ in Fig. 5.

We have also performed the reverse Fourier transform for $h/2e$ oscillations, and the resulting B_{c1} is shown in Fig. 9(c). However, the overall trend seems to be about the opposite of that for h/e (There is no similar correlation for the FT amplitude as a function of V_g in Fig. 5.) This result was a little surprising to us at first, and we do not rule out the possibility of an artifact. But it is also plausible that the trend is an indication of real transport physics. We have discussed the role of backscattering in quenching the h/e oscillations. Now consider the case of large-angle, intraband scattering, if a k is reflected into the $-k$ state in the same subband with phase coherence retained. This kind of scattering kills the h/e oscillation if the scattering takes place either inside the ring or in the ports. But if the scattering occurs in the ports it could *enhance* the $h/2e$ oscillation amplitude, by forcing the electron to make another trip around the ring. So the overall effect of backscattering on $h/2e$ is not necessarily negative. A more detailed study of the roles of specific backscattering mechanisms on different AB oscillation components is necessary.

SUMMARY

We have performed a careful experiment on GaAs/$Al_xGa_{1-x}As$ rings to study the correlation between the $B=0$ subband population and the AB oscillation amplitude at low magnetic fields. Strong correlations are observed between the one-dimensional subband populations and the Fourier amplitude of the oscillations. There is also a correlation with the degree of order in the envelope function as judged through its autocorrelation function. These samples have shown improvements on eliminating most of the impurity scattering, pointing towards the possibility of purely ballistic solid state interferometers. Questions for further theoretical and experimental investigation include whether or not the modes contribute independently to the interference patterns and how classical mechanisms (such as scattering in the port junctions and orbit trapping) affect the envelope function.

ACKNOWLEDGMENTS

This work was supported by IBM and the Microelectronics Center of North Carolina. We thank K. Li, V. Long, and Y. Wang for their assistance during the measurements and D. Kern and S. Rishton for help with lithography.

[1] Y. Aharonov and D. Bohm, Phys. Rev. **115**, 485 (1959).

[2] S. Washburn and R.A. Webb, Rep. Prog. Phys. **55**, 1311 (1992), and references cited therein.

[3] M. Büttiker, Y. Imry, and R. Landauer, Phys. Lett. **96A**, 365 (1983); Y. Gefen, Y. Imry, and M.Ya. Azbel, Phys. Rev. Lett. **52**, 129 (1984); M. Büttiker, Y. Imry, R. Landauer, and S. Pinhas, Phys. Rev. B **31**, 6207 (1985); M. Büttiker, in *SQUID '85*, edited by H.A. Lübbig (de Gruyter, Berlin, 1985); S. Datta, M.R. Melloch, S. Banyopadhyay, and M.S. Lundstrom, Appl. Phys. Lett. **48**, 487 (1986).

[4] Y. Imry, in *Directions in Condensed Matter Physics*, edited by G. Grinstein and E. Mazenko (World Scientific, Singapore, 1986).

[5] D.A. Wharam, M. Pepper, H. Ahmed, J.E.F. Frost, D.G. Hasko, D.C. Peacock, D.A. Ritchie, and G.A.C. Jones, J. Phys. C **21**, L209 (1988); B. van Wees, H. van Houten, C.W.J. Beenakker, J.G. Williamson, L.P. Kouwenhoven, D. vander Marel, and C.T. Foxon, Phys. Rev. Lett. **60**, 848 (1988).

[6] G. Timp, R. Behringer, E.H. Westerwick, and J.E. Cunningham, in *Quantum Coherence and Mesoscopic Systems*, edited by B. Kramer (Plenum, New York, 1991), and references cited therein.

[7] C.W.J. Beenakker and H. van Houten, in *Solid State Physics*, edited by H. Ehrenreich and D. Turnbull (Academic, London, 1991), Vol. 44.

[8] S.E. Ulloa, A. MacKinnon, E. Castaño, and G. Kirczenow, in *Handbook of Semiconductors*, edited by P. Landsberg (North-Holland, Amsterdam, 1992).

[9] G. Timp, A.M. Chang, P. Mankiewich, R. Behringer, J.E. Cunningham, T.Y. Chang, and R.E. Howard, Phys. Rev. Lett. **58**, 2814 (1987); G. Timp, R.E. Behringer, and J.E. Cunningham, Phys. Rev. B **42**, 9259 (1990).

[10] K. Ishibashi, Y. Takagaki, K. Gamo, and S. Namba, Solid State Commun. **64**, 573 (1987); A.M. Chang, K. Owusu-Sekyere, and T.Y. Chang, *ibid.* **67**, 1027 (1988).

[11] C.J.B. Ford, T.J. Thornton, R. Newbury, M. Pepper, H. Ahmed, C.T. Foxon, J.J. Harris, and C. Roberts, J. Phys. C **21**, L325 (1988); C.J.B. Ford, T.J. Thornton, R. Newbury, M. Pepper, H. Ahmed, D.C. Peacock, D.A. Ritchie, J.E.F. Frost, and G.A.C. Jones, Appl. Phys. Lett. **54**, 21 (1989).

[12] G. Timp, P. Mankiewich, P. deVegvar, R. Behringer, J.E. Cunningham, R.E. Howard, H.U. Baranger, and J.K. Jain, Phys. Rev. B **39**, 6227 (1989).

[13] P.G.N. deVegvar, G. Timp, P.M. Mankiewich, R. Behringer, and J.E. Cunningham, Phys. Rev. B **40**, 3491 (1989).

[14] C.J.B. Ford, A.B. Fowler, J.M. Hong, C.M. Knoedler, S.E. Laux, J.J. Wainer, and S. Washburn, Surf. Sci. **229**, 307 (1990); A.M. Chang and T.Y. Chang, Bull. Am. Phys. Soc. **38**, 229 (1993).

[15] K. Ismail, S. Washburn, and K.Y. Lee, Appl. Phys. Lett. **59**, 1998 (1991); K.Y. Lee *et al.*, J. Vac. Sci. Technol B **9**, 2834 (1991).

[16] J. Liu, K. Ismail, K.Y. Lee, J.M. Hong, and S. Wash-

burn, Phys. Rev. B **47**, 13 039 (1993); S. Washburn, K.I. Ismail, and K.Y. Lee, in *Quantum Effect Physics, Electronics and Applications*, edited by K. Ismail, T. Ikoma, and H.I. Smith (Institute of Physics and Physical Society, Bristol, 1992), pp. 153–156.

[17] S. Washburn, H. Schmid, D. Kern, and R.A. Webb, Phys. Rev. Lett. **59**, 1791 (1987).

[18] R. Landauer, Physica **38D**, 226 (1989); M. Büttiker, Phys. Rev. Lett. **65**, 2901 (1990).

[19] B.L. Altshuler and B.Z. Spivak, Pisma' Zh. Eksp. Teor. Fiz. **42**, 363 (1985) [JETP Lett. **42**, 447 (1985)].

[20] A.Yu. Zyuzin and B.Z. Spivak, Zh. Eksp. Teor. Fiz. **93**, 994 (1987) [Sov. Phys. JETP **66**, 560 (1987)].

[21] A. Houghton, J. R. Senna, and S. C. Ying, Phys. Rev. B **25**, 2196 (1982); **25**, 6468 (1982); M. A. Paalanen, D. C. Tsui, and J. C. Hwang, Phys. Rev. Lett. **51**, 2226 (1983).

[22] C.L. Kane and M.P.A. Fisher, Phys. Rev. Lett. **68**, 1220 (1992).

[23] C.G. Smith, M. Pepper, H. Ahmed, J.E.F. Frost, D.G. Hasko, R. Newbury, D.C. Peacock, D.A. Ritchie, and G.A.C. Jones, J. Phys. Condens. Matter **1**, 9035 (1989).

[24] A.D. Stone and Y. Imry, Phys. Rev. Lett. **56**, 189 (1986).